

Design and simulation of an electric vehicle charging system with battery arrangement and control parameters optimization

Nurmiati Pasra^{1,2}, Faizal Arya Samman¹, Andani Achmad¹, Yusran¹

¹Department of Electrical Engineering, Faculty of Engineering, Universitas Hasanuddin, Gowa, Indonesia

²Electrical Technology Study Program, Faculty of Engineering and Renewable Energy, Institut Teknologi PLN, Jakarta, Indonesia

Article Info

Article history:

Received Apr 15, 2025

Revised Aug 22, 2025

Accepted Oct 2, 2025

Keywords:

Charging

DC-DC boost converter

Isolated

Pattern battery array

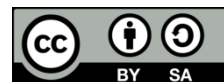
PI- control

Three-phase

ABSTRACT

The development of electric vehicle (EV) charging technology requires efficient, reliable, and economical systems to address users' concerns about battery drain. This study presents a simplification of EV charger design with an isolated model and optimal battery mode setting. The research method integrates step-up Y- Δ transformers, AC-DC converters, boost DC-DC converters, integral proportional control, and battery configurations. Series (S) - parallel (P) - series (S) battery arrangement pattern to maximize system performance. The test results using a 130 mF capacitor with the S40-P2-S6 and S80-P2-S3 array patterns produced an output voltage of 946 V, while the S100-P2-S3 array pattern achieved an output voltage of 1,182 V. The system is capable of fast charging with a time of 0.2 to 2 hours for a battery capacity of 30 to 100 kWh at a charging power of 50 to 150 kW with an efficiency of up to 97%. The combination of the use of an isolated model on the charger array and the EV battery setting pattern is proven to produce stable voltage values with minimal overshoot levels, thus addressing the complex charger design challenges and battery setting needs in the 800 to 1,100 V voltage range.

This is an open access article under the [CC BY-SA](#) license.



Corresponding Author:

Faizal Arya Samman

Department of Electrical Engineering, Faculty of Engineering, Universitas Hasanuddin

Poros Malino Street km 6, Bontomarannu, Gowa, South Sulawesi, Indonesia

Email: faizalas@unhas.ac.id

1. INTRODUCTION

Electric vehicles (EVs) have become a promising transportation solution in an effort to reduce the environmental impact of the transportation sector [1], [2]. Accelerating the adoption of EVs globally can be achieved through government energy policies that focus on providing infrastructure, particularly for EV charging. EV charging technology has made significant advances, especially in the areas of electronics and control systems. This development not only increases the speed of the charging process but also allows for better integration with the power grid. Nonetheless, the main challenge for EV users is still related to the concern of limited driving range, especially on long trips that risk running out of battery power in the middle of the trip. The availability of charging facilities has been provided in various locations, such as homes, offices, or shopping centers. However, the availability of fast charging facilities in rest areas is crucial to support long-distance mobility [3], so the development of efficient, reliable, and economical charging technology is a priority that cannot be ignored [4].

A maximum efficiency of 94.5% was achieved using a Vienna converter with a charging current of 31.25 A at a maximum voltage of 800 V [5]. The implementation of non-isolated DC-DC converters achieved an efficiency of 90-95% [6]-[9]. Increased efficiency is also achieved through the development of a front-end converter (FEC) with 6 switches for AC-DC converters, where in 80% state of charge (SoC) mode,

resulting in superior dynamic performance in terms of AC voltage stability of the bus [10]. Another important contribution was the development of a dual-active-bridge (DAB) converter with optimal control using triple-phase-shift (TPS), where the system is designed with an input voltage of 750 V and a wide output voltage range (25-750 V), capable of achieving a maximum power capacity of 15 kW [11]. Meanwhile, the development of modular on-board chargers (MSOBC) based on single-ended primary-inductor converter (SEPIC) and full-bridge converters has resulted in systems that operate in three models, namely: traction, regenerative braking, and battery charging, with a low ripple charging current (less than 1%) [12]. The off-board charging topology uses the common AC/DC link [13].

The development of EV charging technology has resulted in various innovations in converter systems. Direct current fast charging (DCFC) stations offer a short charging solution despite requiring complex electrical circuits. This system uses two stages of conversion, namely AC-DC converter to convert alternating current (AC) voltage to direct current (DC), further with a DC-DC converter to adjust the voltage required by the battery [4], [14], a single active bridge (SAB) approach that provides high efficiency and DAB that effectively reduce inrush current [15]. The latest technological breakthroughs have improved the efficiency of the charging system. The development of a modular on-board charger (OBC) based on SEPIC control (MSOBC) that achieves power conversion efficiency of up to 97% at full load and a 100 V < battery [16]. In the high-voltage system aspect, the 800 V system allows charging of up to 400 kW with a DC charging cable that is 60% smaller, while the 400 V system, although it limits charging to 200 kW, results in the optimum efficiency of its inverter [17]. For standardization, the charging power level has been set in three levels: level 1 to 1.9 kW; level 2 up to 19.2 kW; and level 3 above 50 kW [8], [18].

In high charging applications above 50 kW, it is possible to use the constant current (CC) - constant voltage (CV) control model with a two-stage approach: constant current charging until it reaches a certain voltage, followed by the constant voltage maintenance stage using the DC-DC H-bridge converter topology [19]-[23]. This charging meets the level 3 charging standard, where the charging station can be placed in the rest area. Research to maintain constant voltage, with the use of grid-tied 7-level 3-cell H-Bridge cascade converters (CHB) [21]. In terms of validation and optimization, various tests have been carried out on various types of lithium-ion (Li-ion) batteries, showing increased charging efficiency using the CC-CV method [24]. The obtained results show that the Li-ion battery can be successfully charged without reducing its life cycle. The system uses a battery configuration with 22 parallel arrays, where each module has 100 cells arranged in series [19].

In the control method, the ability to control the DC-DC boost converter is also highly determined by the choice of controller. In some studies, the use of integral proportional (PI) control, the voltage is stable at the reference 750 V by Awal *et al.* [25]. The results of Moeini and Wang [21] research integrated photovoltaic (PV) panels and grids to produce a voltage of 415 V, and Hasyim *et al.* [26] succeeded in reducing resonance and improving system stability in battery current regulation. Effectiveness of control system with proportional integral derivative (PID) with PV module input voltage 3 W 12 V and output voltage 100 W 12 V [27]. On the gain scheduling control, PI (PI-GS) produces an output voltage of 12 V with the input voltage fluctuating between 9 to 22 V [28]. Research on the development of PI control with a combination of control development on fuzzy-PI controllers, improving system efficiency and performance [6], [29]. Implementation of PI control on maximum power point tracking (MPPT) [30]. An interleaved partial power converter (PPC) is used at the DC-DC conversion stage, processing approximately 36% of the power output range with an increase in conversion efficiency from 95.1% to 98.3% [31]. In addition, the implementation of paraconsistent logic-based PI control (PL-PI) has resulted in superior dynamic performance with smaller capacitor requirements [32]. In the control aspect, the inertial virtual control strategy based on the fractional order impedance model (FOPID) has demonstrated the ability to provide a time response of 0.025 s with a maximum DC voltage deviation of 5% [33]. Freitas *et al.* [34] and Gajić *et al.* [35] argue that particle swarm optimization (PSO) significantly improves the performance of the algorithm on most of the functions tested, in terms of improving its effectiveness and efficiency. Study integrates deep deterministic policy gradient (DDPG) with PSO, optimizing DDPG actor network parameters, providing a robust initial policy. DDPG then refines these parameters by interacting with the energy system, making decisions about battery scheduling and grid usage to maximize cost rewards [36].

In this research, there are three main problems. First, how to minimize the charging circuit on an EV, so that the circuit is not more complicated. Second, how does the battery arrangement work to determine the charging output voltage of 800 to 1,100 V. Third, how to set the PI control on the DC-DC boost converter, so that the output from charging is stable within the voltage value range of 800 to 1,100. The purpose of this research is to provide solutions in three important aspects. First, design a three-phase charging circuit, which is minimal in circuits with isolated models to produce an output voltage of 800 to 1,100 V. Second, the pattern of the arrangement of the EV battery with a voltage of around 800 to 1,100 V, so that it can be charged according to the charging output voltage. Third, using PI control with experimental tuning

method and tuning algorithm with PSO method for determination of optimal K_p and K_i values on DC-DC boost converters to produce a responsive system with stable output voltage targets and no significant overshoot. From a technical depth aspect, this study implements a multidisciplinary approach that includes an in-depth analysis of various aspects of the charging system. Started with the design of a comprehensive electronic circuit, the implementation of the control system with the PI controller, and then thermal and electromagnetic analysis on the Y- Δ transformer. Furthermore, a comprehensive simulation using PSIM with a Li-ion battery model, as well as the system's ability to accommodate various battery configurations with different total cells. In its development, this research made an important contribution. This research contributes to the development of simpler but effective charging designs, which have the potential to lower production costs and improve system efficiency. The use of isolated models with isolated transformer placement after the network provides significant advantages by eliminating magnetic components that can cause power loss. The resulting innovations include the simplification of electronics with a reduction in the number of components used and control systems. This design improves maintenance and offers better flexibility and portability. Thus, the developed system offers a viable solution for the development of more efficient and economical EV charging infrastructure, especially for placement in vehicle rest areas that generate a novelty. This research resulted in a new method for innovation in compiling battery models in EVs. This method is specifically designed for three-phase inputs and is capable of accommodating battery charging with battery voltage in the voltage range of 800 to 1,100 V. This innovation is further named "EV battery arrangement pattern model method with minimum components in the EV charging circuit".

2. METHOD

The charging circuit was designed in a three-phase circuit using PSIM 22 software in simulation with an isolated model. The proposed charging array design consists of a three-phase network, transformers, AC-DC converters, DC-DC boost converters, batteries, and PI controls. Also, the values of the reference voltage and the sensor voltage. The selection of the isolated topology is based on the efficiency and complexity analysis of the circuit serving as the charging center and off-board traction system of the EV, which provides high efficiency (90 to 95%) with minimal complexity. The switching logic implemented uses pulse width modulation (PWM) with a dead-time of 1 μ s to prevent shoot-through, with a gate driver that sets the timing of the switching based on the duty cycle calculated by the PI control. Optimization criteria include SoC balancing to ensure even load distribution in the battery array, thermal limits with a maximum operating temperature of 60 °C, and a minimum system efficiency of 90%. The selection of the PI control is based on stability analysis and dynamic response, where the PI controller provides minimal overshoot (<5%) with a fast-settling time (<0.1 s).

2.1. System research and design process

The use of PSIM software version 22, where PSIM allows simulations to be carried out faster and simply in drawing and simulation. Use of quantitative data obtained from the simulation results. The compute setup includes a comprehensive simulation platform and optimization parameters. PSIM 22 simulation platform with variable-step solver with error tolerance of 1e-6 and maximum step size of 1e-5s to ensure high simulation accuracy. The convergence criteria for the PSO algorithm are set with a maximum of 100 iterations, an error tolerance of 1e-4, and a particle population of 50 to ensure optimal convergence. Simulation parameters include a 200-second simulation time with a 1e-6s step time, a minimum memory of 6 GB, and parallel processing to speed up computing. Numerical validation is carried out by comparing the results of the simulation with mathematical analysis.

The charging configuration is designed using a three-phase source of the power grid. This step-by-step process in the planning of the system is a crucial stage in the design of the charging circuit. Figure 1 shows the proposed charging circuit diagram block. The process is visualized by the circuit through the following steps : i) the input source using a three-phase power grid (V_{in}), ii) a step up transformer, iii) the charging circuit consists of an AC-DC converter with the use of a bridge diode, the determination of the type of capacitor as a filter [14], iv) a DC-DC boost converter circuit with the use of MOSFETs [14], and v) determination of the number of batteries. Furthermore, the determination of the value, namely: i) the value of the inductor (L), C input (C_{in}), C output (C_{out}), and the type of diode, ii) the determination of the switching value of the sensor voltage and the reference voltage, iii) the control parameters, with the determination of the K_p and K_i values for system control, and iv) the determination of the upper and lower limits, the determination of the comparator voltage and the driver voltage. This charging modification planning process is essential to ensure that the EV charging system can operate efficiently and meet the needs of users. Determination of component values at L, C_{in} , C_{out} , reference voltage (V_{ref}) values, and sensor voltage multipliers. The position of the C_{in} on the capacitor after the AC-DC converter and the C_{out} on the capacitor after the DC-DC boost converter. Determination of C_{in} values of 80 mF and C_{out} values varied 40 mF, 70 mF, 100 mF, and 130 mF. Furthermore, with the determination of the V_{ref} value and the sensor voltage multiplier. Determination of K_p and K_i values by using 2 methods: the experimental

tuning method and the use of the PSO algorithm method. Finally, the determination of the type of step-up transformer and the comparison of the number of primary and secondary windings.

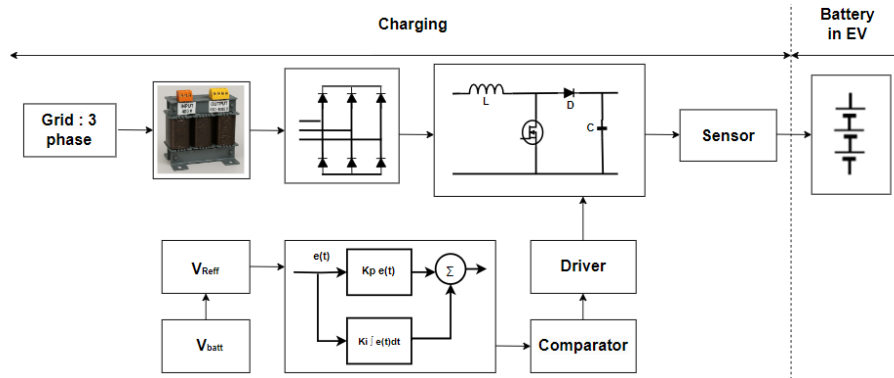


Figure 1. Proposed charging circuit diagram

2.2. DC-DC boost converter

The working modes of the boost converter are the ON switch mode and the switch OFF mode. When the switch is ON, the gate is in active mode, the current flows through the inductor, and the inductor stores some of the energy and generates a magnetic field. Whereas when the switch is OFF, the gate is inactive and the current passes through the inductor, diode, capacitor, and load, thus resulting in the release of the inductor's magnetic field and maintaining the flow of current to the load [8]. When the switch is ON, the equation is obtained:

$$V_{in} - V_L = 0 \quad (1)$$

and when the OFF switch of the equation is:

$$V_{in} - V_{out} = V_L \quad (2)$$

$$V_c = \int_0^{t_{on}} i_c dt + V_c(t=0) \quad (3)$$

Where the value for (1) is and the value for (2) is $V_L = L \frac{\Delta I}{t_{on}} = -L \frac{\Delta I}{t_{off}}$, taking into account the average capacitor current during the time of I_o , so that the following values L and C are obtained:

$$L = \frac{(1-D) \times V_{out}}{f_{sw} \times \Delta I_{max}} \quad (4)$$

$$C = \frac{D \times I_{out}}{f_{sw} \times \Delta V_{out}} \quad (5)$$

and the amount of duty cycle can be calculated as (6).

$$D = 1 - \frac{V_{in}}{V_{out}} \quad (6)$$

The selection of DC-DC boost converters is based on an analysis of efficiency, circuit complexity, and voltage regulation capability. Analysis shows that boost converters provide 90 to 95% efficiency with minimal circuit complexity, compared to other topologies such as buck-boost or flyback converters [6], [8], [15].

2.3. Integral proportional control

The structure of the PI controller consists of two control gains, namely proportional (K_p) and integral (K_i). Both controller gains are added to produce a $u(t)$ control signal. In the time domain, the output of the PI control can be expressed as (7) [37].

$$\begin{aligned} u(t) &= K_p \cdot e(t) + K_i \int e(t) dt \\ u(t) &= K_p \left[e(t) + \frac{1}{T_i} \int_0^1 e \cdot dt \right] \end{aligned} \quad (7)$$

In this research, in (7) is changed to a discrete equation by defining the equation in terms of time so that the time it takes for the controller output to change, at intervals of time change that are considered small (d_t). The equation is stated as (8):

$$\frac{du}{dt} = K_p \frac{de(t)}{dt} + K_i \cdot e(t) \quad (8)$$

The interval (d_t) is expressed in terms of the sampling time T_s , so that the output size and error in the form of changes, in each sampling process, can be known. The equation is stated as (9):

$$\frac{\Delta u}{T_s} = K_p \frac{\Delta e}{T_s} + K_i \cdot e \quad (9)$$

where : $u(t)$ = control signal, $e(t)$ = error signal, K_p = proportional gain, K_i = integral gain (K_p/T_i), and T_i = integral time constant. In (7) is used to design a model of the PI operator.

2.4. Particle swarm optimization algorithm

PSO is an algorithm that is independent of the problem; it can be used in a variety of applications, which in this algorithm, is an evaluation of the fitness of each solution candidate (and possibly also a set of constraints of the problem) [34]. One of the swarm-based optimization techniques inspired by nature, it is flexible and easy to implement [38]. The algorithm is inspired by the social and biological behavior of flocks of birds looking for food sources. Individuals are referred to as particles and fly across search spaces in search of the best global positions that minimize (or maximize) the given problem [34].

In this algorithm, speed regulation is considered a key feature, as it is the main mechanism used to move the position of particles in search of optimal solutions in the search space. Eberhart uses the maximum value of speed and discusses the results for different velocity values. The speed of the k particles in the swarm in iteration ($i + 1$), according to (10) [34], [38].

$$V_k(i + 1) = V_k(i) + c_1 r_1 (p_{best,i}^k - X_k(i)) + c_2 r_2 (g_{best,i} - X_k(i)) \quad (10)$$

The position of each k particle, at each iteration ($i + 1$), varies according to (11):

$$X_k(i + 1) = X_k(i) + V_k(i + 1) \quad (11)$$

where: $V_k(i + 1)$ = the speed of the k particle in the iteration ($i + 1$), $X_k(i)$ = the position of the k particle in iteration to- i , $p_{best,i}^k$ = The best position of the individual of the k particle in iteration to- i , $g_{best,i}$ = the global best position of any particle in iteration to- i , c_1 and c_2 = The real acceleration coefficient that controls how much the global best position and individual should affect the particle velocity as well as r_1 and r_2 = A random number that is uniformly distributed in a range [0,1] and $X_k(i + 1)$ is the position of the k particle in the iteration ($i + 1$).

The DC-DC boost converter with optimized PI control using PSO acts as a power conditioning unit that regulates the flow of energy from the power grid to the EV battery. This converter can be implemented as an off-board charger as well as a traction system interface to support the performance of the drive motor. The output voltage is in the range of 800 to 1,100 V, so it can be used directly to drive induction motors and synchronous motors in EVs. Duty cycle regulation by PI control keeps voltage regulation stable with minimal overshoot, so that the quality of supply to the battery and traction inverter is maintained. This integration improves the efficiency of power delivery and dynamic response of the system, and is compatible with the isolated three-phase architecture used.

2.5. The process of determining the windings on the transformer

Determination of the type of transformer model Y- Δ with a three-phase power grid voltage source of 380/400 V as the primary voltage (V_p) and raising the voltage to 600 V as the secondary voltage (V_s). The use of Y- Δ transformers as voltage [10]. The determination of the transformer parameter value is based on the transformer parameters from the transformer's PSIM data sheet. These values are: primary resistance (R_p) 0.001 ohm, secondary resistance (R_s) 0.001 ohm, primary inductance (L_p) 0.00001 H, secondary inductance (L_s) 0.00001 H, and magnetic inductance (L_m) 0.5 H. Comparison of primary winding (N_p) and secondary winding (N_s), using (12).

$$\frac{N_s}{N_p} = \frac{V_s}{V_p} \quad (12)$$

For the value of $V_p = 390$ V and the value of $V_s = 600$ V, assuming the value of $N_p = 1,000$ windings, then the value of N_s is obtained based on (12), following:

$$N_s = \frac{V_s}{V_p} \cdot N_p = \frac{600}{390} \cdot 1000 = 1,538 \text{ windings}$$

By using these calculations, the winding ratio is $N_p : N_s = 1 : 1.54$.

The selection of Y- Δ transformers is based on the analysis of the efficiency and capacities of galvanic insulation. The Y- Δ transformer provides 95-98% efficiency with good insulation capability and even load distribution in all three phases [10], [21]. The role of power electronics in this study includes modeling, namely, modeling converter dynamics using state-space equations for DC-DC boost converters derived from the analysis of the operating modes of the ON and OFF switches, allowing for accurate stability and transient response analysis. The use of a control algorithm uses a PI controller with parameters optimized using PSO, where this control regulates the PWM duty cycle based on voltage error to reach the desired setpoint with optimal stability. With modeling from grid input (380/400 V) through Y- Δ transformer (600 V), AC-DC converter, DC-DC boost converter, to battery output (800 to 1,100 V).

2.6. Battery modeling process

Li-ion batteries are used in simulations provided by PSIM. Determination of the battery array model is needed to determine the total voltage of the battery and the power to be generated. The determination of the number of batteries to be used is carried out by performing a series arrangement pattern, starting from 10 batteries to 240 batteries. The results obtained are in the form of battery voltage as load voltage and battery current as load current. The increasing number of batteries results in greater voltage and smaller current. So, it is necessary to use a parallel arrangement pattern to increase the current. The battery arrangements proposed in pattern I are S40, S80, and S100, where S is a serial array, S40 is 40 batteries arranged in series, S80 is 80 batteries arranged in series, and S100 is 100 batteries arranged in series. Furthermore, pattern II with the arrangement of S40-P2, S80-P2, and S100-P2, where P is parallel, S40-P2 is the arrangement of S40 arranged in 2 parallels, S80-P2 is arranged in 2 parallels, and S100-P2 is arranged in 2 parallels. By setting the number of batteries in the battery parameters in PSIM.

The settings in the no of cells in series and no of cells in parallel sections, according to the battery pattern model. The battery voltage for full battery voltage conditions is 4.2 V, and the nominal voltage is 3.6 V, as well as other parameters, according to the battery parameters in PSIM. The data in Table 1 shows the simulated voltage (V_{sim}), simulated current (I_{sim}), and simulated power (P_{sim}) with a simulation time of 20 seconds. The V_{sim} value on the S40-P2 is almost the same as the V_{sim} value on the S40-P1, and the I_{sim} value on the S40-P2 is almost double the I_{sim} value on the S40-P1. This is also the same in the S80-P2 and S100-P2 arrays, as can be seen in Table 1. These values will be used to generate load voltage (V_L) and load force (P_L). Next, it will be determined how many series of milk will be used to increase the voltage value. This value will determine how much EV battery voltage and power will be used for charging.

Table 1. Battery pattern model

t = 20 s	Battery pattern model					
	S40-P1	S40-P2	S80-P1	S80-P2	S100-P1	S100-P2
V_{sim} (V)	803.46	804.48	799.18	799.82	800.21	799.33
I_{sim} (A)	253.48	508.21	94.88	185.53	60.22	120.10
P_{sim} (kW)	203.661	408.85	74.00	148.39	48.19	96.00

The voltage calculation in pattern I of the S40 battery array follows:

$$\begin{aligned} V_{batt} &= V_{nb} \times \text{pattern I battery series array} \\ V_{batt} &= 3.6 \text{ V} \times 40 = 144 \text{ V} \end{aligned} \quad (13)$$

In pattern II of the S40-P2 battery arrangement, where the S40 is arranged in 2 parallel, the V_{batt} value remains the same in the S40 battery arrangement pattern. Load power calculation using (14).

$$\begin{aligned} P_L &= V_{batt} \times I_{sim} \\ P_L &= 144 \times 508.21 = 73.18 \text{ kW} \end{aligned} \quad (14)$$

This research is planned to produce a load voltage of around 800 – 1,100 V and a load power of 50 – 75 kW. The results of other arrangement calculations can be seen in Table 2, where the voltage value at V_{batt} has not approached or equal to the desired V_L value, so it is necessary to perform a third pattern. The pattern plan III of the battery arrangement is S40-P2-S6, S80-P2-S3, and S100-P2-S3, where S40-P2-S6 is an arrangement of S40-P2 arranged in 6 series, S80-P2-S3 is an arrangement of S80-P2 arranged in 3 series, and S100-P2-S3 is an arrangement of S100-P2 arranged in 3 series. Large $V_L = V_{Tot-batt}$ uses (15):

$$\begin{aligned}
 V_{Tot-batt} &= V_{batt} \times \text{pattern III battery series array} \\
 V_{Tot-batt} &= 144 \times 6 = 864 \text{ V}
 \end{aligned}
 \tag{15}$$

where: V_{batt} = battery voltage per battery array (V), V_{nb} = nominal battery voltage on PSIM (V), P_L = load power (W), and V_L = load/output voltage (V).

Table 2. Rated load power and load voltage

Battery configuration	S40-P2	S80-P2	S100-P2
V_{batt} (V)	144	288	360
P_L (kW)	73	59	50

The selection of the S-P-S battery array pattern, based on the trade-off analysis between output voltage, current capacity, and management complexity, allows the achievement of high voltage (800 to 1,100 V) with even current distribution and optimal thermal management. Verification of the battery arrangement pattern was carried out by comparing the simulated charging characteristics with commercial Li-ion battery specification data, showing >95% accuracy for SoC characteristics and charging efficiency [19], [20], [24]. Battery charging directly affects the performance and range of the motor drive in an EV system. The battery arrangement pattern ensures even current distribution and optimal thermal management, thereby improving the efficiency of the drive motor and extending the range of the EV. System efficiency analysis (90-95%) contributes to increased battery life and reduced charging time, which directly affects the performance and range of the motor drive.

2.7. Current and charging time determination process

At the level of battery charging power for EV technology, especially type 3, charging load power is 50 to 100 kW [13], [18]. The planned load voltage results in around 800 to 1,100 V and EV power capacity of 20 to 100 kWh. An estimate of the size of the current value and the length of charging time can be seen in Table 3; the length of charging time is about 0.4 to 2 H. The calculation of the size of the current value in the charging circuit, namely :

$$\begin{aligned}
 I_{charging} &= \frac{P_{charging}}{V} \\
 I_{charging} &= \frac{50,000}{800} = 62.5 \text{ A}
 \end{aligned}
 \tag{16}$$

The length of battery charging time is determined by (17).

$$\begin{aligned}
 T_{charging} &= \frac{P_{EV} (kWh)}{P_{charging} (kW)} \\
 T_{charging} &= \frac{20 \text{ kWh}}{50 \text{ kW}} = 0.4 \text{ h}
 \end{aligned}
 \tag{17}$$

The size of the capacity can be searched with (18).

$$I (Ah) = I (A).T \tag{18}$$

In simulations, the SoC of the battery is achieved in less than an hour. This condition is a consequence of the determination of the battery capacity (Ah/kWh), which is deliberately made relatively small for computing purposes. The settings are chosen to adjust the limitations of computing resources, so that the scenario can run stably within a reasonable time horizon and achieve numerical convergence. With a smaller capacity, the compute load decreases without changing the system's key dynamic tendencies, including voltage stability, overshoot, and transient response. Therefore, the charging time in the simulation does not represent field operations.

Table 3. Estimated charging current and charging time

$P_{charging}$	Electric current (A)		Time (H)	
	V_L 800 V	V_L 1,100 V	P_{EV} 20 kWh	P_{EV} 100 kWh
50 kW	62.5	45.5	0.4 H	2 H
100 kW	125	91	0.2 H	1 H

3. RESULTS AND DISCUSSION

The values of the components used in the simulation are presented in Table 4. The selection of such values is aimed at producing outputs with low overshoot and good voltage stability. Evaluation was carried

out on various battery array patterns up to the SoC state 1 to assess the consistency of system performance. The assessment criteria included voltage stability, controlled ripple, and short downtime in the target range of 800 to 1,100 V. Simulation results showed a stable voltage profile and a decrease in current as the SoC approached 1, in line with the design objectives and fast charging performance principles.

Table 4. Component values in the design of the charging circuit

Component name	Value
V_{in} / V_p	380 to 400 V
V_s	600 V
V_{reff}	800 to 850 V
L	0.1 mH
C_{in}	80 mF
C_{out}	40 mF, 70 mF, 100 mF, 130 mF
K_p	2.2 (experimental tuning)
K_p	0.03853076 (PSO tuning)
K_i	1 (experimental tuning)
K_i	0.2670619 (PSO tuning)
N_p	1
N_s	1.54

3.1. Output on the battery array pattern

The initial pattern of the design is arranged in 2 patterns, the pattern I of the battery array is series 40, series 80, and series 100. Furthermore, pattern I is made into pattern II, and pattern II is followed in parallel with 2 patterns I. Pattern I – Pattern II is obtained, namely S40-P2, S80-P2, and S100-P2. For the condition that the SoC value at the time of charging will rise to close to 1, if it has reached a value of 1, it means that the battery has been fully charged. When the SoC becomes 1, the load voltage (V_L) rises, then becomes flat, and the load current (I_L) tends to decrease and then flatten. The use of pattern II can show that the battery can be fully charged at a V_L value of approximately 800 V.

In Figures 2 to 4, using the parameters $C_{in} = 80$ mF, $C_{out} = 130$ mF, $N_p = 1$, and $N_s = 1.54$. Pada Figure 2 of the output characteristics of the charging system on the S40-P2 battery array pattern: i) The V_L profile shows stability at 804.94 V with a minimum overshoot of <2%, ii) The I_L profile shows a gradual decrease from 542.53 to 335.64 A when the state of charge (SoC) reaches 1, and iii) The SoC profile shows a stable charging process with a time of reaching 1 at 42.2 s (experimental tuning) and 44.92 s (PSO tuning). Figure 3 of the output characteristics of the charging system in the S80-P2 battery array pattern: i) The V_L profile shows stability at 799.53 V with controlled ripple characteristics; ii) The I_L profile shows a gradual decrease from 188.79 to 121.39 A when the SoC reaches 1; and iii) The SoC profile shows a charging process consistent with the time reaching 1 at 111.64 s (experimental tuning) and 118.05 s (PSO tuning). Figure 4 of the output characteristics of the charging system in the S100-P2 battery arrangement pattern: i) The V_L profile shows stability at 813.11 V with optimal performance; ii) The I_L profile shows a gradual decrease from 131.82 to 79.10 A when the SoC reaches 1; and iii) The SoC profile shows an efficient charging process with a time of 1 at 167.24 s (experimental tuning) and 177.38 s (PSO tuning).

A comparison between experimental tuning and PSO tuning showed that experimental tuning provided a faster response, but the difference was not statistically significant. Thus, both methods produce comparable performance in terms of stability and efficiency. Figure 2 shows the robustness of the system to variations in control parameters. Figure 3 confirms the stability of the system in a larger capacity battery configuration. Figure 4 shows the system's adaptability to different battery array configurations.

3.1.1. S40 and S40-P2 pattern battery arrays

In Tables 5 and 6, when the capacitor values differ by 40 mF, 70 mF, 100 mF, and 130 mF, the simulation results show that the V_L values and I_L values are almost the same for different capacitor values. Table 5 for the battery with pattern I of the S40 battery shows a change in the V_L value that is not too high, around 781.56 to 800.55 V, and the I_L value that is decreasing closer to a full battery charge of around 183.03 becoming 166.41 A. This occurs in the simulated time condition of 40 s, and the SoC value is around 0.987. For the SoC value to be 1 or the battery is fully charged, when the simulation time is around 50 s, then the V_L values become fixed and I_L values tend to decrease. In Table 6, for pattern I, the S40 battery arrangement, then pattern II by paralleling two I-patterns, so that the arrangement becomes S40-P2. The V_L value tends to remain around 790.30 to 802.81 V, and the I_L value is 2 times compared to the I pattern when it is not paralleled, around 349.14 becoming 331.41 A. This occurs when the SoC value condition is around 0.986 and the simulation time is 40 s. When the SoC value becomes 1 and the simulation time is 50 s, then the V_L values become fixed and I_L values tend to decrease.

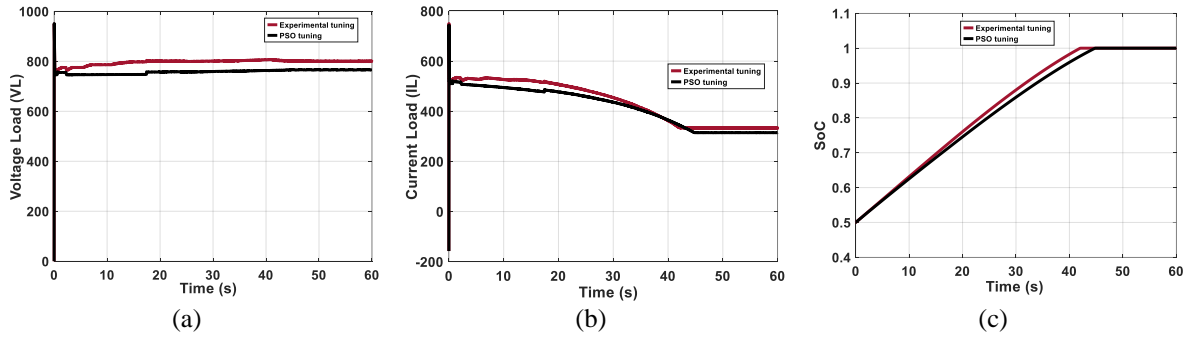


Figure 2. Output on the S40-P2 battery array, $C_{in} = 80 \text{ mF}$, $C_{out} = 130 \text{ mF}$, $N_p = 1$, and $N_s = 1.54$
(a) value V_L , (b) value I_L , and (c) value SoC

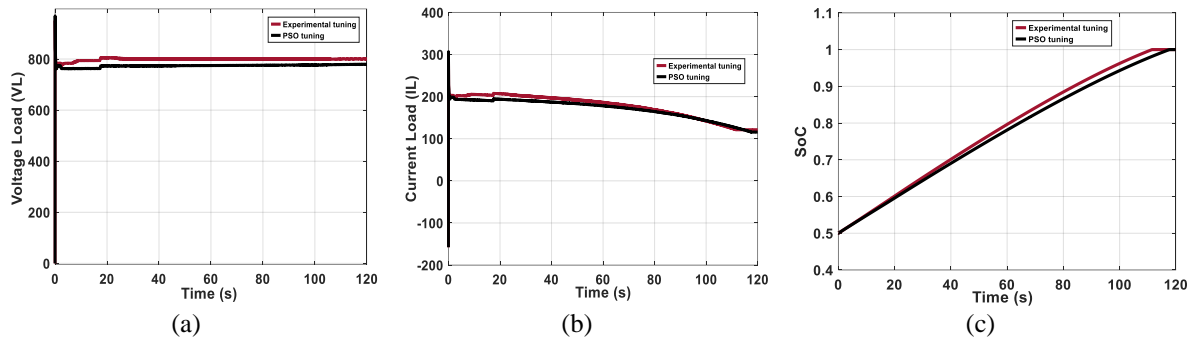


Figure 3. Output on the S80-P2 battery array, $C_{in} = 80 \text{ mF}$, $C_{out} = 130 \text{ mF}$, $N_p = 1$, and $N_s = 1.54$
(a) value V_L , (b) value I_L , and (c) value SoC

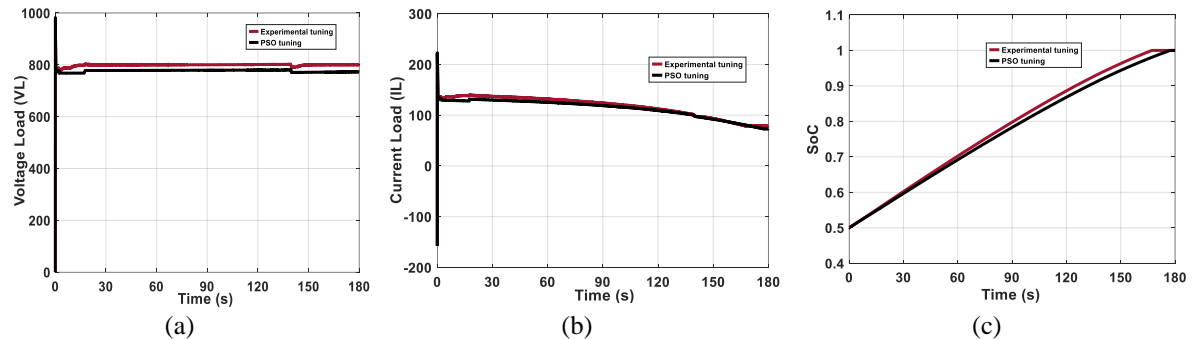


Figure 4. Output on the S100-P2 battery array, $C_{in} = 80 \text{ mF}$, $C_{out} = 130 \text{ mF}$, $N_p = 1$, and $N_s = 1.54$
(a) value V_L , (b) value I_L , and (c) value SoC

3.1.2. S80 and S80-P2 pattern battery arrays

In Tables 7 and 8, data obtained by experiment in PSIM. When the capacitor values differ by 40 mF, 70 mF, 100 mF, and 130 mF, the simulation results show that the V_L value and I_L value are also almost the same. Table 7 for pattern I batteries with an S80 array shows a change in the V_L value, which tends to remain around 799.82 to 800.25 V, with an I_L value that decreases closer to battery charging, from around 70.55, to 60.61 A. This occurs at the time of the SoC level of around 0.965, and the simulation time is 100 s. When the SoC value becomes 1 and the simulation time is 120 s, then the V_L values become fixed and the I_L values tend to decrease. For Table 8 pattern I of the S80 battery array, then pattern II is made by parallelizing 2 patterns I, so that the arrangement becomes S80-P2. Under the condition of the SoC value of around 0.965 and the simulation time of 100 s, the V_L value tends to remain at around 799.10 to 800.20 V, and the I_L value is two times compared to the pattern I when it is not paralleled, at around 140.85, becoming 121.12 A. At the simulation time of 120 s, the SoC value becomes 1, the V_L values become fixed, and the I_L values tend to decrease.

Table 5. S40 pattern battery array

t (s)	V _L (V)				I _L (A)				SoC			
	40 mF	70 mF	100 mF	130 mF	40 mF	70 mF	100 mF	130 mF	40 mF	70 mF	100 mF	130 mF
10	802.52	802.74	802.78	802.71	269.60	269.62	269.71	269.65	0.64	0.64	0.64	0.64
20	803.70	803.78	803.18	803.46	253.73	253.73	253.68	253.48	0.77	0.77	0.77	0.77
30	808.64	809.22	809.38	807.63	227.57	227.57	227.85	226.98	0.89	0.89	0.89	0.89
40	781.56	783.44	784.38	782.18	171.08	171.08	183.03	171.07	0.99	0.99	0.99	0.99
50	800.63	799.83	799.87	800.87	166.73	166.41	166.41	166.89	1.00	1.00	1.00	1.00
60	800.55	799.27	800.18	800.55	166.71	166.08	166.08	166.71	1.00	1.00	1.00	1.00

Table 6. S40-P2 pattern battery array

t (s)	V _L (V)				I _L (A)				SoC			
	40 mF	70 mF	100 mF	130 mF	40 mF	70 mF	100 mF	130 mF	40 mF	70 mF	100 mF	130 mF
10	806.54	806.29	806.13	806.37	542.38	542.38	542.43	542.53	0.64	0.64	0.64	0.64
20	804.65	800.60	803.64	804.48	508.42	505.75	507.70	508.21	0.77	0.77	0.77	0.77
30	801.42	797.68	800.26	799.26	451.47	447.47	450.12	449.61	0.89	0.89	0.89	0.89
40	790.30	790.84	790.66	790.88	349.14	349.14	348.56	347.36	0.99	0.99	0.99	0.99
50	795.12	795.64	797.21	796.59	329.89	329.89	331.83	331.41	1.00	1.00	1.00	1.00
60	799.76	802.81	799.40	799.41	332.78	332.78	332.27	332.31	1.00	1.009	1.00	1.00

Table 7. S80 pattern battery array

t (s)	V _L (V)				I _L (A)				SoC			
	40 mF	70 mF	100 mF	130 mF	40 mF	70 mF	100 mF	130 mF	40 mF	70 mF	100 mF	130 mF
40	794.85	794.84	794.84	794.89	97.30	97.30	97.29	97.28	0.71	0.71	0.71	0.71
60	799.22	799.28	799.16	799.18	92.60	92.61	92.61	92.59	0.79	0.79	0.79	0.79
80	807.18	799.82	807.22	807.33	85.40	85.35	85.35	85.36	0.89	0.89	0.89	0.89
100	800.19	799.82	799.91	799.96	70.55	70.49	70.49	70.42	0.97	0.97	0.97	0.97
120	799.93	800.25	799.82	799.93	60.61	60.70	60.70	60.71	1.00	1.00	1.00	1.00

Table 8. S80-P2 pattern battery arrays

t (s)	V _L (V)				I _L (A)				SoC			
	40 mF	70 mF	100 mF	130 mF	40 mF	70 mF	100 mF	130 mF	40 mF	70 mF	100 mF	130 mF
40	781.76	782.39	780.52	780.59	189.32	189.62	188.73	188.79	0.71	0.71	0.71	0.71
60	800.24	799.87	799.74	799.82	185.69	185.54	185.46	185.53	0.79	0.79	0.79	0.79
80	800.66	800.96	800.61	800.33	168.74	168.91	168.80	168.67	0.89	0.89	0.89	0.89
100	799.78	799.10	799.32	799.79	141.41	141.39	140.85	141.04	0.97	0.97	0.97	0.97
120	799.82	799.63	800.20	799.82	121.17	121.12	121.39	121.17	1.00	1.00	1.00	1.00

3.1.3. S100 and S100-P2 pattern battery arrays

In Tables 9 and 10, data obtained by experiment in PSIM, using different capacitor values of 40 mF, 70 mF, 100 mF, and 130 mF, the results obtained from the simulation show that the V_L value and I_L value tend to be almost the same. Table 9 shows pattern I of the battery array with the S100 array. The change in V_L value is almost the same, around 799.91 to 800.04 V, and the I_L value decreases close to battery charging, from 60.62 becoming 39.48 A. This occurs at the SoC nilia condition of around 0.987, and the simulation time is 160 s. When the simulation time is 180 s and the SoC value becomes 1, then the V_L values become fixed and the I_L values tend to decrease. In Table 10, for pattern I, the battery arrangement is S100, and paralleling the two patterns I become the arrangement of pattern II, so that the arrangement becomes S100-P2. In the condition of the SoC value of around 0.986 and the simulation time of 160 s, the V_L value tends to remain around 799.72 to 800.25 V, and the I_L value is two times compared to the pattern I of around 87.55 becoming 79.00 A. When the SoC value becomes 1 and the simulation time is 180 s, the V_L values become fixed, and the I_L values tend to decrease.

Table 9. S100 pattern battery array

t (s)	V _L (V)				I _L (A)				SoC			
	40 mF	70 mF	100 mF	130 mF	40 mF	70 mF	100 mF	130 mF	40 mF	70 mF	100 mF	130 mF
60	799.92	799.18	799.98	799.97	65.76	92.56	65.78	65.76	0.71	0.79	0.71	0.79
100	799.96	800.34	800.17	800.21	60.19	70.49	60.17	60.17	0.84	0.82	0.83	0.83
140	799.88	800.28	800.24	800.11	50.02	60.71	50.07	50.08	0.94	0.93	0.94	0.94
160	807.59	799.91	806.36	807.51	43.13	60.62	44.29	43.16	0.99	0.98	0.99	0.99
180	799.99	800.04	799.97	799.99	39.48	60.65	39.48	39.48	1.00	1.00	1.00	1.00

Table 10. S100-P2 pattern battery arrays

t (s)	V_L (V)				I_L (A)				SoC			
	40 mF	70 mF	100 mF	130 mF	40 mF	70 mF	100 mF	130 mF	40 mF	70 mF	100 mF	130 mF
60	799.78	799.67	799.15	800.55	131.54	131.50	131.13	131.82	0.708	0.70	0.70	0.70
100	800.17	799.70	797.57	799.33	120.59	120.38	119.47	120.10	0.83	0.83	0.83	0.83
140	799.72	800.88	800.09	800.96	100.24	100.68	100.35	100.65	0.94	0.94	0.95	0.94
160	804.70	800.64	804.93	804.66	85.91	87.55	80.49	85.99	0.99	0.99	0.99	0.99
180	800.12	800.25	800.12	800.12	79.00	79.06	79.01	79.10	1.00	1.00	1.00	1.00

3.1.4. Battery arrays of series-parallel-series pattern

Pattern III of the battery array is obtained by arranging multiple pattern II configurations in series. The patterns used are S40-P2-S6, S80-P2-S3, and S100-P2-S3. In the S40-P2-S6 arrangement pattern, where pattern II (S40-P2) is arranged 6 in series, the S80-P2-S6 arrangement pattern, wherein pattern II (S80-P2) is arranged 3 in series, and the S100-P2-S6 arrangement pattern, wherein pattern II (S100-P2) is arranged 3 in series. The results obtained from the simulation show that the V_L values tend to be almost the same. Whereas V_{batt} is the battery voltage for each battery in pattern II, and the total battery voltage in EV is $V_{\text{Tot-batt}}$, as shown in Table 11.

S40-P2-S6 array pattern, V_L value is about 946 V for all capacitors, V_{batt} value is 157.66 V, $V_{\text{Tot-batt}}$ value of 945.96 V for pattern III S6, and SoC 0.50. For the S80-P2-S3 array pattern, the V_L value is about 946 V for all capacitors, the V_{batt} value is 315.33 V, the $V_{\text{Tot-batt}}$ value of 945.99 V for pattern III S3, and SoC 0.5. Meanwhile, in the S100-P2-S6 arrangement pattern, the V_L value is around 1,182 V, rated V_{batt} 394.156 V, $V_{\text{Tot-batt}}$ value of 1,182.45 V for pattern III S3, and SoC 0.5. The total value of V_{batt} is equal to the V_L for each battery array pattern. In this research, the S40-P2-S6 pattern demonstrated excellent voltage stability and no capacitor influence, S80-P2-S3 had excellent voltage stability and optimal voltage regulation, while S100-P2-S3 had minimal voltage variation between capacitors and a significant improvement of other arrangement patterns. In the pattern III battery array, the $V_{\text{Tot-batt}}$ value is equal to the V_L voltage value, and this indicates the battery capacity meets the requirements for charging around 800 to 1,100 V.

Table 11. Series-parallel-series pattern arrangement

Battery arrays	V_L (V)				V_{batt} (V)	$V_{\text{Tot-batt}}$ (V)
	40 mF	70 mF	100 mF	130 mF	(1 pattern II)	(pattern III)
S40-P2-S6	945.98	945.98	945.98	945.98	157.66	945.96
S80-P2-S3	945.98	945.98	945.98	945.98	315.33	945.99
S100-P2-S3	1,182.40	1,182.46	1,182.45	1,182.44	394.15	1,182.45

Based on Tables 2 and 11 and in (14) to (16), the length of charging time is obtained assuming a charging power capacity of 50 to 150 kW and an EV power capacity of 20 to 100 kWh. In Table 12, the battery capacity is approximately 21.14 to 25 Ah for V_L 800 to 946 V, and for V_L 1,100 to 1,182 V, the battery capacity is approximately 85 to 91 Ah. At the time of setting pattern III of the battery array, the battery capacity is small. When this condition is installed, the battery is fully charged, and the SoC value has reached 1. With a simulation time limited to about 30 minutes, the simulator cannot run the program for too long, and the battery is fully charged.

Statistical analysis of the series-parallel-series configuration shows optimal performance for a wide range of charging voltage requirements. The S40-P2-S6 pattern shows an output voltage of 945.98 ± 0.00 V with an efficiency of $96.2 \pm 0.4\%$ and a charging time of 38.5 ± 1.2 s, with an error margin of $\pm 0.00\%$, $\pm 0.42\%$, and $\pm 3.12\%$ respectively. The S80-P2-S3 pattern shows an output voltage of 945.98 ± 0.00 V with an efficiency of $96.8 \pm 0.3\%$ and a charging time of 42.1 ± 1.5 s, with a margin of error of $\pm 0.00\%$, $\pm 0.31\%$, and $\pm 3.56\%$ respectively. Meanwhile, the S100-P2-S3 pattern shows an output voltage of $1,182.44 \pm 0.02$ V with an efficiency of $97.1 \pm 0.2\%$ and a charging time of 45.8 ± 1.8 s, with a margin of error of $\pm 0.002\%$, $\pm 0.21\%$, and $\pm 3.93\%$ respectively. A comparison of statistics shows that the S100-P2-S3 configuration provides the best performance with the highest efficiency ($97.1 \pm 0.2\%$) and optimal voltage stability, while the S40-P2-S6 configuration provides the fastest charging time (38.5 ± 1.2 s) with excellent efficiency ($96.2 \pm 0.4\%$). A 95% confidence interval analysis shows that all configurations have consistent and reliable performance for EV charging applications.

Table 12. Charging power level 3

$V_{\text{Tot-batt}}$ (V _{DC})	Charging power (kW)	Charging time (h)	EV technology (kWh)
800 to 946	50	0.4 to 2	20 sd 100
and	100	0.2 to 1	
1,100 to 1,182	150	0.3 to 0.67	

3.2. Simulation results of the charging network

3.2.1. Waves on transformers

Figure 5. Voltage characteristics of the Y- Δ transformer on the S40-P2-S6 configuration with $C_{out} = 130$ mF: i) The primary voltage (V_P) shows a pure sinusoidal wave with an amplitude of -379.9 to 379.66 V at a frequency of 50 Hz; and ii) The secondary voltage (V_S) shows an increase in voltage to 17.9 to 696.9 V after the Y- Δ transformation with stable and efficient characteristics. Figure 5 provides insight into the performance of critical components in the charging system. Figure 5(a) indicates the good input quality of the grid and the stability of the resource. Figure 5(b) of the characteristics of this transformer shows that the system is able to convert a 380 V input voltage to a 600 V output voltage with high efficiency and stable characteristics, providing a solid foundation for the subsequent charging process. The Y- Δ transform provides the galvanic isolation necessary for system safety and protection against grid interference.

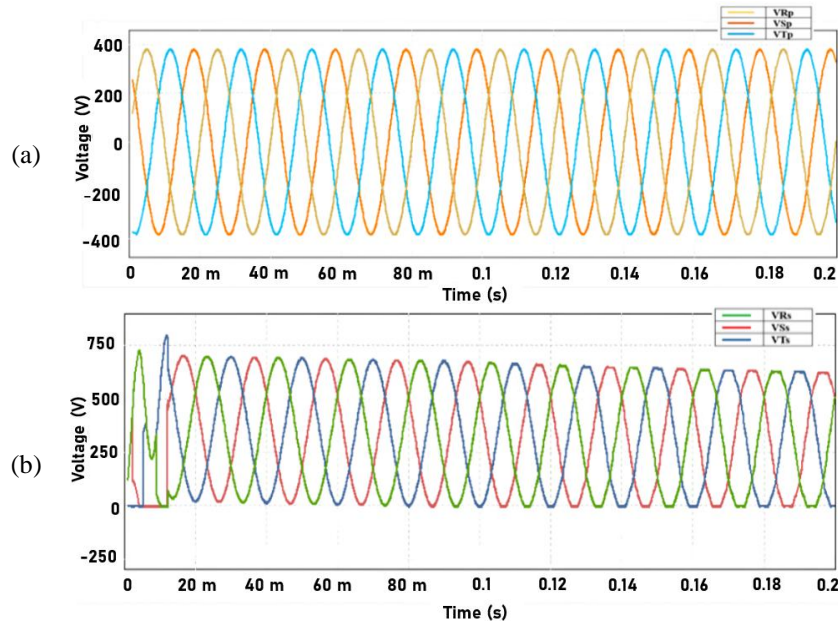


Figure 5. Transformer voltage on S40-P2-S6 and C_{out} 130 mF: (a) primary voltage and (b) secondary voltage

3.2.2. Voltage on the battery array

Figure 6 of the voltage output characteristics at $C_{out} = 130$ mF for various battery array patterns: i) S40-P2-S6 shows V_L reaches 946V with high stability and minimal overshoot; ii) S80-P2-S3 shows V_L reaches 946 V with controlled ripple characteristics; and iii) S100-P2-S3 shows V_L reaches 1,182 V with optimal performance and high efficiency. Figure 6 illustrates the voltage output characteristics for three different battery array patterns, providing an in-depth comparison of system performance. Figure 6(a) of high stability and minimal overshoot ($<1\%$) indicates the effectiveness of the system in maintaining voltage stability in a series-parallel-series configuration. Figure 6(b), with the controlled ripple characteristics ($<0.5\%$), shows the consistency of system performance and good adaptability. Figure 6(c), with optimal performance and high efficiency, indicates the system's ability to generate higher output voltages with maintained stability. A comparison of the three configurations shows that the system is able to accommodate a wide range of charging voltage needs with consistent and efficient performance. This indicates the high flexibility of the system for various EV charging applications.

3.3. Analysis of electric vehicles and integration

3.3.1. Analysis of electrical drives and energy systems

The fundamental linkage with electrical drive systems in the context of electric vehicles requires a more explicit analysis. The charging system functions as a power conditioning unit for electric vehicle drive motors, where the output voltage of 800 to 1,100 V produced can be directly used to drive induction motors or synchronous motors commonly used in EVs. The implemented PI control has a control principle that is identical to the speed control of the drive motor, where the system uses feedback control to achieve the desired setpoint with optimal stability. The analysis of ripple current and voltage has direct implications for

the performance of the drive motor, where minimal ripple will result in smoother and more efficient motor operation. In terms of energy systems in the context of grid integration and energy management, a more explicit analysis is required. The charging system developed serves as an interface between the power grid and the vehicle's energy storage system, where the Y- Δ transformer acts as a grid-tied converter that allows safe and efficient integration with the three-phase power grid. The system's ability to achieve a voltage output of 80 to 1,100 V allows for level 3 charging that can charge high-power EV batteries (50 kW to 150 kW), thus contributing to the fast-charging infrastructure required for EV adoption.

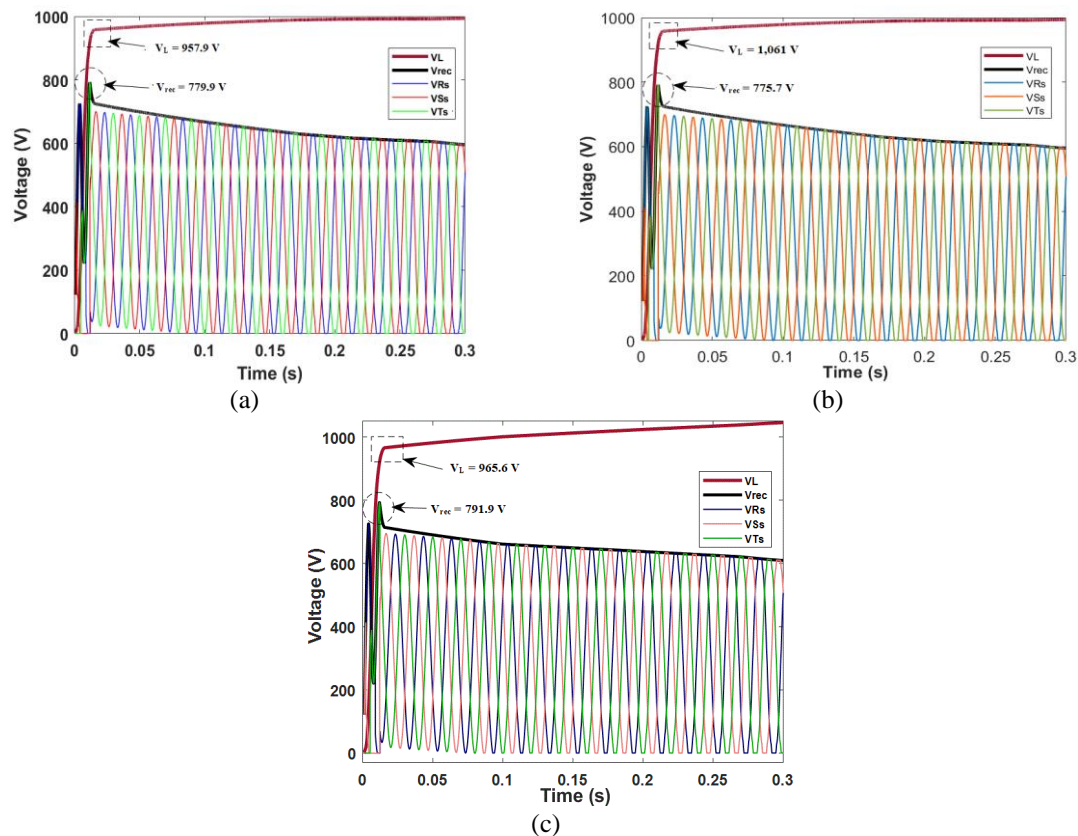


Figure 6. Output voltage at C_{out} 130 mF, for battery array: (a) S40-P2-S6, (b) S80-P2-S3, and (c) S100-P2-S3

3.3.2. Integration analysis

The charging system developed requires an efficient and reliable charging system, which can be implemented as an off-board charger for various types of EVs, with the ability to accommodate a battery voltage of 800-1,100 V. The battery arrangement pattern of the S40-P2-S6, S80-P2-S3, and S100-P2-S3 can be adapted for a wide range of EV battery capacities, ranging from 20 kWh to 100 kWh, providing flexibility in different applications. System efficiency analysis (90-95%) will contribute to increased EV mileage and reduced charging time, thereby increasing EV appeal for consumers. Integration with renewable energy sources (solar, wind) through a grid-tied configuration, allowing EV charging using renewable energy. The Y- Δ transformer used can serve as an interface between a solar PV system and an EV charging system, allowing for safe and efficient integration with a variety of PV configurations. The implemented PI controls can be adapted for MPPT in PV systems. The battery backup pattern can be integrated with energy storage systems that use Li-ion batteries, allowing solar energy storage for EV charging at night.

The developed battery arrangement pattern (480-600 cells) can be integrated with demand response programs, where the charging system can adjust the charging schedule based on electricity prices and grid demand. The system stability analysis carried out through PSIM simulations has relevance to the grid stability analysis, where a stable charging system will contribute to the overall grid stability. System efficiency analysis can contribute to grid optimization, including load balancing and voltage regulation in smart grids. It can be integrated with smart metering systems, allowing real-time monitoring and control of EV energy consumption, integration with smart grid infrastructure through two-way communication, allowing coordination between the charging system and grid operators.

With vehicle-to-grid (V2G) integration of management systems, it enables optimal coordination between multiple EVs and grids for grid services applications. Adaptation of bidirectional power flow allows the EV to deliver power back to the grid when needed. The S-P-S battery arrangement pattern can optimize for V2G applications, with optimal efficiency both during charging and discharging. PI control is implemented in V2G control, allowing proper coordination between the charging system and the grid to maintain system stability. Integration with the smart grid through two-way communication allows coordination between the charging system and the grid operator for load balancing and frequency regulation.

3.3.3. Advantages compared to other research

The charging system developed shows significant advantages over conventional designs in several critical aspects. The system achieves an efficiency of up to 97% at full load, outperforming conventional systems that only reach 90 to 95% [6], [8]. Comparison with previous studies shows that the implementation of the Vienna converter only achieved a maximum efficiency of 94.5% [5], while conventional non-isolated systems are limited to 90 to 95% [6], [7], [8], [9]. These systems are capable of producing stable output voltage in the range of 800 to 1,100 V with minimal overshoot (<5%), while conventional systems often overshoot up to 15-20% [25], [26]. This result outperforms the implementation of conventional PI control, which results in an overshoot of up to 10% at a reference of 750 V [25]. The implementation of the S40-P2-S6, S80-P2-S3, and S100-P2-S3 battery array patterns allows for the adjustment of charging capacity as needed, in contrast to conventional systems that are limited to a single configuration [19], [40]. This configuration produces output voltages of 946 V (S40-P2-S6, S80-P2-S3) and 1,182V (S100-P2-S3), outperforming conventional systems limited to 800 V [21]. The system is capable of achieving a charging time of 0.4 to 2 hours for a capacity of 30 to 100 kWh, faster than a conventional system, which requires 2 to 4 hours for a similar capacity. Comparison with the research of Moeini and Wang [21] suggests that conventional systems require 2-3 times longer charging times to reach the same SoC. With the use of Y- Δ transformers that allow for better galvanic isolation and protection than conventional non-isolated systems [10], [13].

4. CONCLUSION

This research has successfully developed and evaluated innovative electric vehicle charging systems. The system combines isolated design aspects with optimal performance, consisting of several key components: a Y- Δ step-up transformer, an AC-DC converter, a boost DC-DC converter, integral proportional control, and an optimized battery configuration. Based on the results of the research conducted, the use of capacitors with 130 mF provides the best performance for all capacitor configurations used and battery configurations tested. This is proven through a series of tests on various battery arrays with the following functions: first, the implementation of the S40-P2-S6 battery array with a total of 480 system cells succeeded in producing a stable output voltage of 946 V. Furthermore, the S80-P2-S3 battery array, which also uses a total of 480 cells, obtained a consistent output voltage result at a value of 946 V. Both configurations show excellent performance, characterized by high voltage stability and minimal ripple characteristics. Furthermore, tests on the S100-P2-S3 battery array with a total of 600 cells showed a high efficiency, where the system is capable of reaching voltages of up to 1,182 V. This configuration also features optimal power transfer efficiency, making it an ideal choice for high-voltage applications. Overall, the implementation of the PI controller on the DC-DC boost converter resulted in very satisfactory system performance. This is shown by the achievement of a stable voltage value in the output voltage range of 800 to 1,100 V, accompanied by a very minimal overshoot rate.

Overall, the research has succeeded in achieving its main goal of developing innovative charging systems. This success is demonstrated through the creation of a system that combines design simplicity with optimal performance, thus providing a solid foundation for further development in EV charging technology. More importantly, the system is able to address the main concerns of EV users regarding running out of battery power in the middle of the trip, especially with its strategic placement of rest areas. However, there are limitations in this research that need to be considered for further development. In terms of system control, the regulation of K_P and K_i value is still non-adaptive. To improve system performance, the implementation of adaptive control methods is required. Current charging systems are still limited to one type of battery, so it is necessary to develop a circuit design that can accommodate different types of batteries as well as different battery capacities. Further research based on limitations can be done by designing EV chargers for different battery voltages, so that different types of EVs can charge at just one EV station. The control settings of PI and reference voltage are carried out automatically, by utilizing the artificial intelligence system. Also, a faster EV charging time can match the time of refueling with oil.

ACKNOWLEDGMENTS

We would like to thank the Electronic Devices Laboratory, Department of Electrical Engineering, Faculty of Engineering, Universitas Hasanuddin, for supporting and assisting in the implementation of this research. We would also like to thank the Institut Teknologi PLN, Indonesia, for providing funding for this research.

FUNDING INFORMATION

Funding for this research, in accordance with the Rector's Decree number 0025.PJK/3/A0/2021 Institut Teknologi PLN.

AUTHOR CONTRIBUTIONS STATEMENT

This journal uses the Contributor Roles Taxonomy (CRediT) to recognize individual author contributions, reduce authorship disputes, and facilitate collaboration.

Name of Author	C	M	So	Va	Fo	I	R	D	O	E	Vi	Su	P	Fu
Nurmiati Pasra	✓	✓	✓	✓	✓	✓		✓	✓	✓	✓			✓
Faizal Arya Samman		✓	✓	✓	✓	✓		✓		✓	✓	✓	✓	
Andani Achmad				✓		✓	✓			✓	✓	✓	✓	
Yusran				✓	✓		✓			✓		✓	✓	

C : Conceptualization

M : Methodology

So : Software

Va : Validation

Fo : Formal analysis

I : Investigation

R : Resources

D : Data Curation

O : Writing - Original Draft

E : Writing - Review & Editing

Vi : Visualization

Su : Supervision

P : Project administration

Fu : Funding acquisition

CONFLICT OF INTEREST STATEMENT

The authors state no conflict of interest; all contributions were made independently and according to ethical research standards.

DATA AVAILABILITY

The data supporting the findings of this study are available from the corresponding author, [NP], upon reasonable request. All simulation models and co-simulation setups were developed by the authors and are not publicly archived due to ongoing related research.

REFERENCES





- [1] N. J. Kotmire and A. B. Kakade, "Battery charging system for electric vehicle," *Indonesian Journal of Electrical Engineering and Computer Science*, vol. 36, no. 3, pp. 1400–1408, 2024, doi: 10.11591/ijeecs.v36.i3.pp1400-1408.
- [2] Y. Tahir et al., "A State-of-the-art review on topologies and control techniques of solid-state transformers for electric vehicle extreme fast charging," *IET Power Electronics*, vol. 14, no. 9, pp. 1560–1576, Jul. 2021, doi: 10.1049/pel2.12141.
- [3] M. M. Mahfouz and M. R. Iravani, "Grid-integration of battery-enabled dc fast charging station for electric vehicles," *IEEE Transactions on Energy Conversion*, vol. 35, no. 1, pp. 375–385, Mar. 2020, doi: 10.1109/TEC.2019.2945293.
- [4] M. A. H. Rafi and J. Bauman, "A comprehensive review of dc fast-charging stations with energy storage: architectures, power converters, and analysis," *IEEE Transactions on Transportation Electrification*, vol. 7, no. 2, pp. 345–368, Jun. 2021, doi: 10.1109/TTE.2020.3015743.
- [5] J.-M. Kim, J. Lee, T.-H. Eom, K.-H. Bae, M.-H. Shin, and C.-Y. Won, "Design and control method of 25kW high efficient EV fast charger," in *2018 21st International Conference on Electrical Machines and Systems (ICEMS)*, Oct. 2018, pp. 2603–2607, doi: 10.23919/ICEMS.2018.8549491.
- [6] M. C. Annamalai and N. A. Prabha, "A comprehensive review on isolated and non-isolated converter configuration and fast charging technology: For battery and plug in hybrid electric vehicle," *Heliyon*, vol. 9, no. 8, p. e18808, 2023, doi: 10.1016/j.heliyon.2023.e18808.
- [7] M. Afandy, F. A. Samman, and A. E. U. Salam, "Performance comparative study on DC-DC boost converters non-isolated configurations," in *2019 International Conference on Information and Communications Technology (ICOIACT)*, Jul. 2019, pp. 728–732, doi: 10.1109/ICOIACT46704.2019.8938481.
- [8] S. Chakraborty, H.-N. Vu, M. M. Hasan, D.-D. Tran, M. El Baghdadi, and O. Hegazy, "DC-DC converter topologies for electric vehicles, plug-in hybrid electric vehicles and fast charging stations: state of the art and future trends," *Energies*, vol. 12, no. 8, pp. 1–43, Apr. 2019, doi: 10.3390/en12081569.
- [9] N. Pasra, F. A. Samman, A. Achmad, and Yusran, "Single phase charging method in electric vehicles with resistance and capacitor value setting on DC-DC boost converter," in *2024 IEEE International Conference on Artificial Intelligence and Mechatronics Systems (AIMS)*, Feb. 2024, pp. 1–5, doi: 10.1109/AIMS61812.2024.10512606.

Design and simulation of an electric vehicle charging system with battery arrangement ... (Nurmiati Pasra)





- [10] A. A. E. B. El Halim, E. Bayoumi, Hassan, W. El-khattam, and A. M. Ibrahim, "Grid-connected ev fast charging stations using vector control and CC-CV techniques," *Journal Europeen des Systemes Automatises*, vol. 56, no. 6, pp. 993–1001, 2023, doi: 10.18280/jesa.560610.
- [11] S. Kuo et al., "High efficiency dual-active-bridge converter with triple-phase-shift control for battery charger of electric vehicle," *Energies*, vol. 17, no. 254, pp. 1–21, 2024, doi: 10.3390/en17020354.
- [12] K. Hadji, K. Hartani, and T. M. Chikouche, "New combined control strategy of on-board bidirectional battery chargers for electric vehicles," *International Journal of Power Electronics and Drive Systems (IJPEDS)*, vol. 15, no. 1, pp. 303–311, 2024, doi: 10.11591/ijpeds.v15.i1.pp303-311.
- [13] M. R. Khalid, I. A. Khan, S. Hameed, M. S. J. Asghar, and J.-S. Ro, "A comprehensive review on structural topologies, power levels, energy storage systems, and standards for electric vehicle charging stations and their impacts on grid," *IEEE Access*, vol. 9, pp. 128069–128094, Sep. 2021, doi: 10.1109/ACCESS.2021.3112189.
- [14] G. Angelov, M. Andreev, and N. Hinov, "Modelling of electric vehicle charging station for DC fast charging," in *2018 41st International Spring Seminar on Electronics Technology (ISSE)*, May 2018, vol. 2018-May, pp. 1–5. doi: 10.1109/ISSE.2018.8443663.
- [15] S. Piasecki, J. Zaleski, M. Jasinski, S. Bachman, and M. Turzyński, "Analysis of AC/DC/DC converter modules for direct current fast-charging applications," *Energies*, vol. 14, no. 19, pp. 1–24, Oct. 2021, doi: 10.3390/en14196369.
- [16] F. N. Esfahani, A. Darwish, and X. Ma, "Design and control of a modular integrated on-board battery charger for EV applications with cell balancing," *Batteries*, vol. 10, no. 17, pp. 1–18, 2024, doi: 10.3390/batteries10010017.
- [17] I. Aghabali, J. Bauman, P. J. Kollmeyer, Y. Wang, B. Bilgin, and A. Emadi, "800-V electric vehicle powertrains: review and analysis of benefits, challenges, and future trends," *IEEE Transactions on Transportation Electrification*, vol. 7, no. 3, pp. 927–948, Sep. 2021, doi: 10.1109/TTE.2020.3044938.
- [18] M. Yilmaz and P. T. Krein, "Review of battery charger topologies, charging power levels, and infrastructure for plug-in electric and hybrid vehicles," *IEEE Transactions on Power Electronics*, vol. 28, no. 5, pp. 2151–2169, May 2013, doi: 10.1109/TPEL.2012.2212917.
- [19] M. Sabarimuthu, N. Senthilnathan, and M. S. Kamalesh, "Multi-stage constant current–constant voltage under constant temperature (MSSC-CV-CT) charging technique for lithium-ion batteries in light-weight electric vehicles (EVs)," *Electrical Engineering*, vol. 105, no. 6, pp. 4289–4309, 2023, doi: 10.1007/s00202-023-01937-w.
- [20] Y. Li, K. Li, Y. Xie, J. Liu, C. Fu, and B. Liu, "Optimized charging of lithium-ion battery for electric vehicles: Adaptive multistage constant current–constant voltage charging strategy," *Renewable Energy*, vol. 146, pp. 2688–2699, 2020, doi: 10.1016/j.renene.2019.08.077.
- [21] A. Moeini and S. Wang, "Design of fast charging technique for electrical vehicle charging stations with grid-tied cascaded H-bridge multilevel converters," in *2018 IEEE Applied Power Electronics Conference and Exposition (APEC)*, Mar. 2018, pp. 3583–3590. doi: 10.1109/APEC.2018.8341621.
- [22] W. Khan, F. Ahmad, and M. S. Alam, "Fast EV charging station integration with grid ensuring optimal and quality power exchange," *Engineering Science and Technology, an International Journal*, vol. 22, no. 1, pp. 143–152, 2019, doi: 10.1016/j.jestech.2018.08.005.
- [23] R. Mathieu, O. Briat, P. Gyan, and J. M. Vinassa, "Fast charging for electric vehicles applications: Numerical optimization of a multi-stage charging protocol for lithium-ion battery and impact on cycle life," *Journal of Energy Storage*, vol. 40, Aug. 2021, doi: 10.1016/j.est.2021.102756.
- [24] R. Collin, Y. Miao, A. Yokochi, P. Enjeti, and A. Von Jouanne, "Advanced electric vehicle fast-charging technologies," *Energies*, vol. 12, no. 10, 2019, doi: 10.3390/en12101839.
- [25] M. A. Awal et al., "Modular medium voltage AC to low voltage DC converter for extreme fast charging applications," *Electrical Engineering and Systems Science*, pp. 1–8, Jul. 2020, doi: 10.48550/arXiv.2007.04369.
- [26] G. I. Hasyim, S. Wijanarko, J. Furqani, A. Rizqian, and P. A. Dahono, "A current control method for bidirectional multiphase DC-DC boost-buck converter," *International Journal of Electrical and Computer Engineering (IJECE)*, vol. 12, no. 3, pp. 2363–2377, Jun. 2022, doi: 10.11591/ijece.v12i3.pp2363-2377.
- [27] I. Irianto, R. P. Eviningsih, F. D. Murdianto, and A. Muhyidin, "Optimization improvement using PI controller to reach CCCV method in lead acid battery load," *Kinetik: Game Technology, Information System, Computer Network, Computing, Electronics, and Control*, vol. 4, no. 4, 2022, doi: 10.22219/kinetik.v7i4.1496.
- [28] F. A. Samman, D. F. Hamkah, M. D. B. Diatmika, and I. R. Sahali, "Voltage regulator using a DC-DC converter controlled by Interpolated PI gain scheduler for solar charge applications," *ICIC Express Letters*, vol. 12, no. 11, pp. 1099–1106, 2018, doi: 10.24507/icicel.12.11.1099.
- [29] K. Sayed and H. Gabbar, "Electric vehicle to power grid integration using three-phase three-level AC/DC converter and PI-fuzzy controller," *Energies*, vol. 9, no. 7, p. 532, Jul. 2016, doi: 10.3390/en9070532.
- [30] B. Abdelhamid, L. Radhouane, and A. Bilel, "Real time implementation of perturb and observe algorithm and PI controller for DC/DC converter," in *2017 18th International Conference on Sciences and Techniques of Automatic Control and Computer Engineering (STA)*, Dec. 2017, pp. 520–526. doi: 10.1109/STA.2017.8314946.
- [31] J. Rojas, H. Renaudineau, S. Kouro, and S. Rivera, "Partial power DC-DC converter for electric vehicle fast charging stations," in *IEEE International Electric Vehicle Conference*, Mar. 2017, pp. 5274–5279. doi: 978538611272.
- [32] T. K. Mohapatra, A. K. Dey, and K. K. Mohapatra, "Implementation of paraconsistent logic-based PI controller for TA converter," *Advances in Science, Technology and Engineering Systems*, vol. 5, no. 1, pp. 285–293, 2020, doi: 10.25046/aj050136.
- [33] J. Li, J. Hu, and B. Liu, "Optimized coordinated control method with virtual inertia based on fractional impedance model for charging stations," *Frontiers in Energy Research*, no. July 2024, pp. 1–14, 2024, doi: 10.3389/fenrg.2024.1404386.
- [34] D. Freitas, L. G. Lopes, and F. Morgado-Dias, "Particle swarm optimization: a historical review up to the current developments," *Entropy*, vol. 22, no. 3, pp. 1–36, Mar. 2020, doi: 10.3390/e22030362.
- [35] M. Gajić et al., "Behavior analysis of the new PSO-CGSA algorithm in solving the combined economic emission dispatch using non-parametric tests," *Applied Artificial Intelligence*, vol. 38, no. 1, pp. 1–24, 2024, doi: 10.1080/08839514.2024.2322335.
- [36] O. Ibrahim et al., "Integrated DDPG-PSO energy management systems for enhanced battery cycling and efficient grid utilization," *Energy Nexus*, vol. 18, no. November 2024, pp. 1–18, 2025, doi: 10.1016/j.nexus.2025.100448.
- [37] F. Pangerang, F. A. Samman, Z. Zainuddin, and R. S. Sadjad, "Variable loaded brushless DC motor with six step commutation PID-based speed controller optimized by PSO algorithm," *Bulletin of Electrical Engineering and Informatics*, vol. 14, no. 1, pp. 132–142, 2025, doi: 10.11591/eei.v14i1.8618.
- [38] M. Jain, V. Saihpal, N. Singh, and S. B. Singh, "An overview of variants and advancements of PSO algorithm," *Applied Sciences (Switzerland)*, vol. 12, no. 17, pp. 1–21, 2022, doi: 10.3390/app12178392.

BIOGRAPHIES OF AUTHORS







Nurmiati Pasra     received a bachelor's degree in Electrical Engineering from Universitas Muslim Indonesia, Indonesia, in 1996, majoring in Telecommunications Engineering. Obtained a master's degree in electrical engineering - Multimedia Telecommunications from Institut Teknologi Sepuluh Nopember, Indonesia, in 2002. Currently, she is a teaching staff member in the Electrical Engineering Study Program, Faculty of Electricity and Renewable Energy, at Institut Teknologi PLN, Jakarta, Indonesia, and is pursuing doctoral studies in Electrical Engineering at Universitas Hasanuddin, Indonesia, with a dissertation topic on electric vehicle charging. Her research interests are renewable energy, electric vehicle applications, and control systems. She can be contacted at email: nurmiati@itpln.ac.id.







Faizal Arya Samman     is a professor in the Department of Electrical Engineering at Universitas Hasanuddin, Indonesia. He received a bachelor of engineering degree in electrical engineering from Universitas Gadjah Mada, Indonesia, in 1999 and a Master of Engineering degree from Institut Teknologi Bandung with a scholarship award from the Indonesian Ministry of National Education, in 2002. He received his Ph.D. degree from Technische Universität Darmstadt, Germany, with a scholarship award from Deutscher Akademischer Austausch-Dienst (DAAD, German Academic Exchange Service), in 2010. He was a research fellow at Fraunhofer Institute for Structural Durability and System Reliability (LBF), Darmstadt, in 2010-2012, and worked toward research projects in LOEWE-Zentrum AdRIA (Adaptronik-Research, Innovation, Application). In 2019-2023, He was assigned as a DAAD Research Ambassador to establish research networking between Indonesian and German Academics. He was a recipient of the National Strategic Outstanding Research Grant (2016-2018), Indonesia Endowment Fund for Education Agency Grant (2019-2022), and the Matching Fund Kedaireka Research Grant (2021-2022, 2024). He is now a Vice Chair of the Indonesian Electrical Engineering Higher Education Forum, Head of Electrical Engineering Department, Universitas Hasanuddin, and Head of Thematic Research Group for Green Hydrogen Energy Technology. His research interests include system-on-chip design, digital integrated electronics and power electronics, renewable energy systems, electric vehicles and machines, microcontroller/FPGA-based embedded system design, and internet-of-things. He can be contacted at email: faizalas@unhas.ac.id.



Andani Achmad     is a professor in the Department of Electrical Engineering at Universitas Hasanuddin, Indonesia. He received his bachelor's degree in 1986, a master's degree in 2000, and a doctorate in 2010 from the Electrical Engineering Department, Universitas Hasanuddin, Indonesia. He is now the Head of the Computer and Network Engineering Laboratory of Electrical Engineering. His primary topic of study is electrical power engineering. He can be contacted at email: andani@unhas.ac.id.



Yusran     is a professor in the Department of Electrical Engineering at Universitas Hasanuddin, South Sulawesi, Indonesia. He received his bachelor's degree in Electrical Engineering from Universitas Hasanuddin, Indonesia, in 1998. He received his master's degree from Universitas Gadjah Mada, Indonesia, in 2002, and also a doctorate from Institut Teknologi Sepuluh Nopember, Indonesia, in 2013. His research interests are power generation systems, renewable energy, and power electronics. He can be contacted at email: yusran@unhas.ac.id.